3D Submillimeter-Resolution Reduced-Field-of-View Diffusion Tensor Imaging

A. T. Van[1], J. Holtrop[2], and B. P. Sutton[2]
[1]Electrical and Computer Engineering, University of Illinois at Urbana-Champaign, Urbana, IL, United States, [2]Bioengineering, University of Illinois at Urbana-Champaign, Urbana, IL, United States

Introduction

For better delineation of neuronal architecture, higher spatial resolution is always desirable. Challenges in realization of high spatial resolution include but are not limited to long total scan time, low signal-to-noise ratio (SNR), and high sensitivity to T2* blurring, off-resonance, and motion-related artifacts. In the present work, the reduced field-of-view (rFOV) imaging approach is chosen for minimizing the effects of the previously mentioned artifacts at high resolution. Three-dimensional encoding in combination with multiecho acquisition is proposed for increased SNR efficiency (the ratio between SNR and the square root of the total acquisition time) as compared to traditional 2D rFOV acquisitions. Imperfections in realization of rFOV imaging are minimized by the proposed penalized iterative reconstruction algorithm.

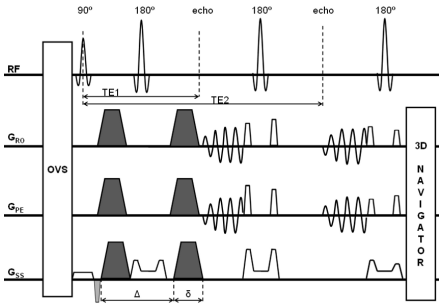

Fig. 1: Schematic sequence timing.

Method

rFOV with 3D encoding and multiecho acquisition:

Outer volume suppression (OVS) [1] is used in the current study for rFOV imaging because it has the advantages of no TE increase, compatibility to multislab acquisition [2], and simple implementation. 3D encoding is done using a stack of multishot variable density spiral trajectory [3]. To reduce the total scan time, two second refocusing pulses are used to acquire two echoes per every repetition of the sequence (Fig. 1). A third refocusing pulse is applied after the acquisition of the second echo to acquire a 3D navigator necessary for estimation and correction of the motion induced phase error. The 3D navigator is a gradient-recalled stack of single-shot constant density spirals [4].

Due to the imperfection of the slab-selection profile and the inconsistent motion-induced phases, later echoes in a multiecho diffusion-weighted acquisition suffer from attenuation beyond T2 decay [5]. Phase cycling of the refocusing pulses can help stabilize the echo signals [5, 6] for a multiecho sequence with long echo train length (more than four). Since the current echo train length is three, we seek to improve the echo train signal by enlarging the slab selection thickness of the refocusing pulses as compared to the desired slab thickness [6, 7]. Phantom results in Fig. 2 show the improvement of the echo train attenuation as the slab thickness of the refocusing pulses increases. Diffusion-weighted acquisition has smaller echo train attenuation because the large diffusion gradients act effectively as spoilers, destroying unwanted echo paths that interfere with the desired signal.

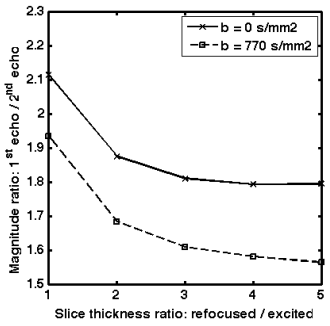

Fig. 2: Reduction of echo train attenuation as a function of refocusing slab thickness increase.

Penalized iterative reconstruction:

Due to the imperfections of the regional saturation pulses, residual signals exist outside of the desired FOV that cannot be modeled if we choose to reconstruct only the rFOV. To incorporate the incompleteness of the regional saturation pulses into the system modeling, we propose to reconstruct the full FOV image at the cost of being ill-conditioned. Regularization using an energy penalty on the region outside of the rFOV improves the condition of the reconstruction problem. The cost function of the proposed iterative reconstruction algorithm is:

$$\Psi(\mathbf{x}_{full}) = \left\|\mathbf{y} - \mathbf{A}\mathbf{x}_{full}\right\|^2 + \beta\left\|\mathbf{x}_{full}(mask)\right\|^2, \qquad (1)$$

where $\mathbf{x}_{full}$ is the full FOV image, $\mathbf{y}$ is the phase corrected *k*-space data, $\mathbf{A}$ is the Fourier encoding matrix on the 3D trajectory after motion-induced phase error correction [8], β is the penalty weight, and *mask* is the mask of the outside of the rFOV of interest.

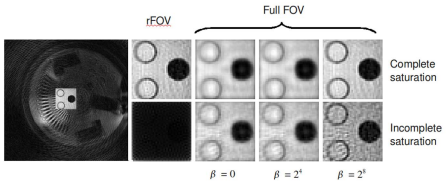

Fig. 3: Comparison between rFOV reconstruction and the proposed full FOV reconstruction.

Data Acquisition:

In vivo data were acquired using Siemens 3 T Trio scanner with a 12-channel head coil on a healthy subject in accordance with the institutional review board. The obtained resolution was 0.8 x 0.8 x 1 mm^3 with 4 x 4 x 2 cm^3 FOV on the human pons. Other imaging parameters were: TE1 = 59 ms, TE2 = 99 ms (for data), TE3 = 160 ms (for navigator), b = 770 s/mm^2, and 11 diffusion-encoding directions. The acquisition was cardiac-gated for minimizing pulsation effects, resulting in an effective TR of two R-R intervals (approximately 2 s). The total acquisition time is 22 minutes.

Results

Simulation: Fig. 3 shows the comparison of the reconstruction results obtained with rFOV reconstruction, and full FOV reconstruction with different penalty weights for both the complete and incomplete saturation cases. When the saturation is complete (as shown on the leftmost panel), rFOV reconstruction gives a high resolution image well matched with the numerical phantom. When the saturation is incomplete, rFOV reconstruction fails to give a reasonable image due to model mismatch. At proper penalty weight (in this case = 2^8), full FOV reconstruction generates high resolution results even in the case of incomplete saturation.

In vivo: Fig. 4 shows three planes (coronal, sagittal, axial) of the obtained color-coded FA maps of the human pons at 0.8 x 0.8 x 1 mm^3 resolution. Unlike 2D rFOV, the proposed acquisition gives high resolution in 3D, enabling the delineation of the pons both in-plane and through-plane.

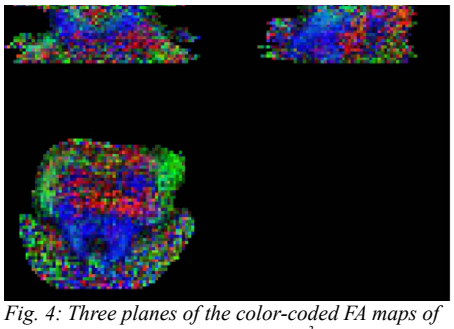
Fig. 4: Three planes of the color-coded FA maps of the human pons at 0.8 x 0.8 x 1 mm^3.

Conclusion

The current study shows that 3D rFOV with multiecho acquisition is a promising technique for achieving 3D submillimeter resolution DTI *in vivo* of a localized neuronal structure.

References [1] Wilm et al, MRM. 57: 625-630, 2007; [2] Van et al, ISMRM 2010, p.1618; [3] Kim et al, MRM. 50: p.214-219, 2003; [4] Glover, MRM. 42:p412-415, 1999; [5] Roux, JMR. 155: p278-292, 2002, [6] Sarlls et al, MRM. 60:, p.270-276, 2008; [7] Pell et al., JMRI. 23: p-248-252, 2006; [8] Van et al., ISMRM 2009, p. 1391.

Acknowledgements – This work was supported by an AFAR research grant**.**